DIELECTRIC MEASUREMENTS AND MODELING OF SNOW IN THE 3- TO 37-GHz RANGE

Martti Hallikainen, Helsinki University of Technology, Radio Laboratory, Finland
Fawwaz T. Ulaby, University of Michigan, Radiation Laboratory, Ann Arbor
Mohammed Abdelrazik, E-Systems, Inc., Greenville, Texas

ABSTRACT

Microwave dielectric measurements of dry and wet snow were made at nine frequencies between 3 GHz and 18 GHz and at 37 GHz using two free-space transmission systems. The measurements were conducted during the winters of 1982 and 1983 in Lawrence, Kansas. The following parametric ranges were covered: (a) liquid water content: 0 to 12.3% by volume, (b) snow density: 0.09 to 0.42 g/cm^3, (c) temperature: 0 to -5°C, and -15°C (scattering loss measurements), and (d) crystal size: 0.5 to 1.5 mm. The experimental data indicate that the dielectric behavior of wet snow follows closely the dispersion behavior of water. For dry snow, volume scattering is the dominant loss mechanism at 37 GHz. The applicability of several empirical and theoretical mixing models was evaluated using the experimental data. The Debye-like semi-empirical model and the theoretical Polder and Van Santen mixing model were found to adequately describe the dielectric behavior of snow. The Polder and Van Santen model provided a good fit to the measured values of the real and the imaginary part of wet snow only when the shape of water inclusions in snow was assumed to be nonsymmetrical and to depend on snow water content.

1.0 INTRODUCTION

Dry snow is a mixture of ice particles and air voids. After the snow is deposited, the numerous ice particle shapes are modified by metamorphism. Thermodynamically, the ice crystals seek equilibrium for which the ratio of surface area to volume is minimum [1]. Any water in the snowpack collects at points of contact between the grains. The geometry and porosity of snow at high and low liquid water contents have been examined by Colbeck [2]. He concluded that snow, like any porous material, has two distinct regimes of liquid saturation. In the lower range of liquid saturation, the pendular regime, air is continuous throughout the pore space, and the liquid occurs as isolated inclusions. In the higher range of liquid saturation, the funicular regime, the liquid is continuous throughout the pore space and the air occurs in distinct bubbles trapped at narrow constrictions in the pores. There is a sharp transition between the two regimes.

The melt-freeze metamorphism changes the microstructure of snow. The grains become rounded during the melting process, and some of the smaller grains disappear completely. When the water freezes, the snow increases in density and has a greater continuity in the resulting ice matrix. Snow which has undergone several melt-freeze cycles tends to form multiple clusters.

Electromagnetically, a snow medium, in general, is a three-component dielectric mixture consisting of air, ice particles, and liquid water. Both ice and water exhibit dispersion spectra; however, the relaxation frequency for ice is in the kilohertz

range, while that for water at 0°C is about 9 GHz [3]. The complex dielectric constants of ice (low-loss material) and water (high-loss material) depend on frequency and temperature. Consequently, the dielectric constant of snow is, in general, a function of frequency, temperature, volumetric water content, snow density, the shape of ice particles, and the shape of water inclusions.

Several investigations have been conducted over the past few years to evaluate the use of microwave remote sensing systems for determining the extent, water equivalent, and liquid water content of snow cover. Passive measurements of snowpacks have been made in the 5- to 94-GHz range [4-7]. Active measurements have been reported for frequencies between 1 GHz and 36 GHz [5,8]. The measurements include data for both dry and wet snow conditions. Radiometric observations at 18 GHz and 37 GHz, provided by Nimbus-7, have been employed for snow studies both on a global and a regional scale [9,10].

The above-mentioned studies indicate that the frequency range of both active and passive remote sensing measurements and utilization of the available data have been extended to millimeter wavelengths. However, the basic tool for interpreting these data, namely the microwave dielectric properties of snow, are known with satisfactory accuracy only for frequencies below 13 GHz. In fact, as shown in Table 1, only a few microwave dielectric measurements of snow have been made to date. They include only two multifrequency investigations, namely a study of wet snow between 4 GHz and 12 GHz [14], and one for dry snow at four frequencies between 0.8 GHz and 13 GHz [15]. Linlor's sample preparation involved mixing liquid water at 0°C with dry snow [14], which rendered the water distribution in the mixture different in shape from that in natural snow.

Modeling of the microwave dielectric properties of snow is naturally limited to the frequency range of existing experimental studies. Mixing models that assume wet snow to consist of either dry snow and water or, more fundamentally, of air, ice, and water have been applied by several investigators [11,16-19]. Because of the lack of wideband dielectric data for natural snow, the capability of these models to satisfactorily describe the microwave dielectric behavior of dry and wet snow is still open.

This study presents the results of dielectric measurements made over the 3- to 18-GHz range and at 37 GHz for natural dry and wet snow. Several empirical and theoretical models are applied to fit the experimental data. Additionally, a study of scattering losses in dry and wet snow is included.

2.0 MEASUREMENT TECHNIQUES

Two free-space transmission systems, one operating between 3 GHz and 18 GHz [20] and the other operating at 37 GHz [21], were used for the snow dielectric measurements. The free-space technique is practical for producing data over a wide frequency range, because the same sample can be measured over the entire range. In addition, the free-space technique allows for rapid measurement of wet snow samples, thus preserving the properties of the samples. The two free-space systems were located in an unheated truck when the measurements were conducted. The temperature inside the truck was 0 ± 2°C for measurements of wet snow samples and well below 0°C for measurements of dry snow samples.

2.1 Free-Space Transmission Technique

3- to 18-GHz System

The block diagram of the system is shown in Figure 1. The antenna separation is 23 cm and the sample diameter is 30 cm. Two methods are used to account for multiple reflections within the measurement system. A pulley system is used to vary the sample location between the horn antennas during the measurement of phase shift, and swept-frequency loss measurements are used to record and average reflections. The maximum loss that the present 3- to 18-GHz system can measure is 40 dB.

The complex transmission coefficient for a sample is measured by comparing the amplitude and phase readings of the network analyzer/phase-gain indicator for the sample holder when it is empty and when it is filled with a snow sample:

$$T_m = |T_m| \, e^{j\phi_m} = \frac{(1 - R^2) \, e^{-\gamma d}}{1 - R^2 \, e^{-2\gamma d}}, \quad (1)$$

where γ is the complex propagation constant for the sample and is defined in terms of the attenuation coefficient α and the phase coefficient β as

$$\gamma = \alpha + j\beta, \tag{2}$$

where

$$\alpha = \frac{2\pi}{\lambda_0} \sqrt{\frac{\varepsilon'}{2} \left(\sqrt{1 + \left(\frac{\varepsilon''}{\varepsilon'}\right)^2} - 1\right)} \tag{3}$$

$$\beta = \frac{2\pi}{\lambda_0} \sqrt{\frac{\varepsilon'}{2} \left(\sqrt{1 + \left(\frac{\varepsilon''}{\varepsilon'}\right)^2} + 1\right)} \tag{4}$$

The electric field reflection coefficient is denoted by R and the sample thickness by d. The complex dielectric constant of the sample is $\varepsilon = \varepsilon' - j\varepsilon''$.

The expressions for the magnitude $|T_m|$ and the phase ϕ_m of the transmission coefficient T_m are coupled nonlinear functions of α and β, and hence of ε' and ε''. Therefore, an iterative procedure was used to obtain ε' and ε'' [20].

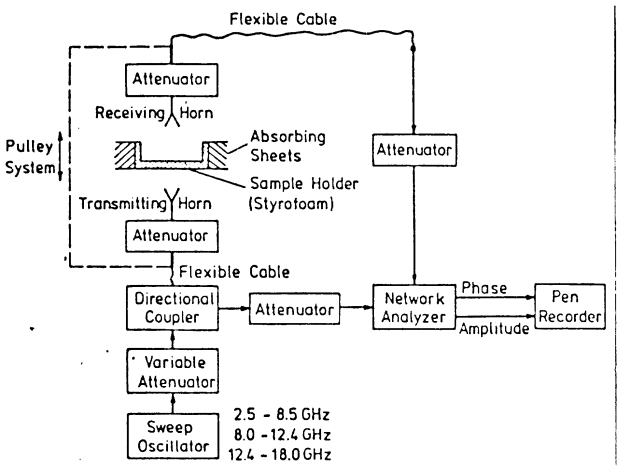

Fig. 1. Block diagram of the 3- to 18-GHz free-space transmission system.

37-GHz System

The block diagram of the measurement system is shown in Figure 2. The antenna separation is 37 cm and the sample diameter is 30 cm (same sample as for the 3- to 18-GHz system). The measurement procedure for this system is different from that for the 3- to 18-GHz system. During the loss measurement, the reference arm is blocked out by a variable attenuator. The sample loss is obtained by measuring the transmitted power without the sample and with the sample inserted. A frequency sweep from 37 GHz to 38 GHz is employed to record and eliminate multiple reflections. The maximum loss that the present 37-GHz system can measure is 40 dB.

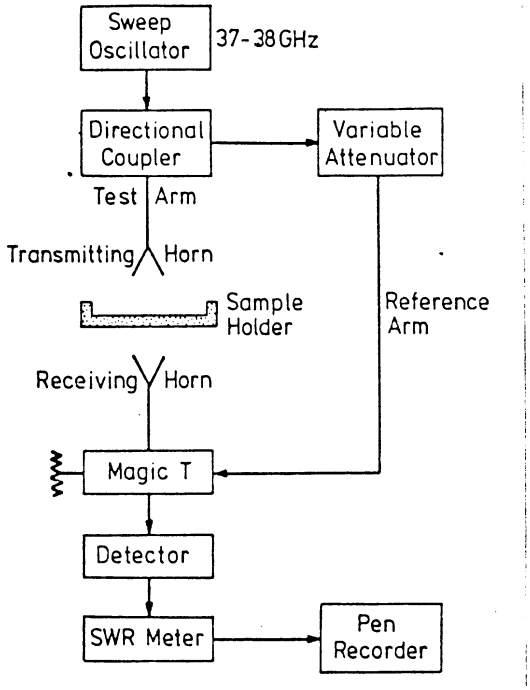

Fig. 2. Block diagram of the 37-GHz free-space transmission system.

Instead of measuring the phase shift due to the sample at a fixed frequency, the interference pattern between 37 GHz and 38 GHz is recorded. The interference is a result of splitting the signal between the reference arm and the test arm and of recombining it again. Due to the phase shift from the sample the interference pattern is shifted in frequency. The frequencies corresponding to the maximum amplitude of the interference pattern without the sample, f_1, and with the sample inserted, f_2, are observed.

The real part of $\sqrt{\varepsilon}$ can be computed from those frequencies and the geometry of the measurement system [21]:

$$\text{Re}\ \sqrt{\varepsilon} = 1 + \frac{\lambda_{02}}{d}\left[L_r\left(\frac{1}{\lambda_{r2}} - \frac{1}{\lambda_{r1}}\right) - L_t\left(\frac{1}{\lambda_{t2}} - \frac{1}{\lambda_{t1}}\right)\right] - \frac{s}{d}\left(\text{Re}\ \sqrt{\varepsilon_s} - 1\right). \tag{5}$$

In Equation (5), L_r and L_t are the lengths of the reference arm and the test arm, respectively, and λ_i refers to wavelength at frequency f_i ($i = 1$ or 2). Subscript r refers to the reference arm and subscript t to the test arm. The thickness and the complex dielectric constant of the sample holder are designated by s and ε_s, respectively.

From the measured values for loss L ($L = |1/T_m|$) and Re $\sqrt{\varepsilon}$, ε' and ε'' can be computed using an iteration process as described in [21].

2.2 Measurement Accuracy and Precision

Measurement accuracy depends upon the measurement technique used and the dielectric properties and the dimensions of the sample. For wet snow samples, the preservation of the sample properties (especially liquid water content) during the measurement is important.

3- to 18-GHz System

In order to determine the absolute precision of the system, test samples ranging from polymethyl methacrylate (low-loss material) to distilled water (high-loss material) were measured [20]. The average deviation over the 3-18 GHz range from previously observed values was for polymethyl methacrylate ($\varepsilon = 2.60 - j0.015$ at 3 GHz, $\varepsilon = 2.57 - j0.0082$ at 25 GHz [22]): 1.2% for ε' and 0.02 dB for the loss; and for distilled water ($\varepsilon = 77.1 - j11.6$ at 3 GHz, $\varepsilon = 43.2 - j33.0$ at 18 GHz for T = 23°C [3]): 2.1% for ε' and 2.8% for ε''. The accuracy of the 3- to 18-GHz system is not sufficient for measurement of the loss of dry snow samples.

The total calculated worst-case error bounds for the measurement of wet snow samples are shown in Figure 3. The samples represent an upper limit (m_v = 12%), a lower limit (m_v = 1.6%, and a medium value (m_v = 5.6%) for the snow sample liquid water content by volume in this study. The thickness of the sample is increased with decreasing water content in order to increase the sample loss and, consequently, the accuracy of the measurement. These error bounds include uncertainties both in the free-space transmission system and in the interpretation of measurements.

The 3- to 18-GHz free-space system was tested against a 4- to 6-GHz waveguide transmission system at 6 GHz using loamy soil samples. The results in Figure 4 show a good agreement between the two systems.

37-GHz System

The 37-GHz system was tested with the same test materials as used for the 3- to 18-GHz system. For polymethyl methacrylate ($\varepsilon = 2.57 - j0.0082$ at 25 GHz [22]) the deviation from previously reported values was 1.5% for ε' and 25% for ε'', whereas for distilled water ($\varepsilon = 19.6 - j29.5$ at 37.5 GHz [3]) the corresponding value was 1.0% for both ε' and ε''. The increase in the accuracy of ε'' is due to the high loss (L > 30 dB) for the water sample compared with that for the polymethyl methacrylate sample (L = 1 dB).

The total error bounds for the measurement of wet snow samples were calculated considering the uncertainties both in the measurement system and the reading accuracy. For water contents $m_v \geq 5.6\%$, the worst-case error bounds for ε' and ε'' are 4% and 5%, respectively. For m_v = 1.6%, they are 4% and 8%, respectively.

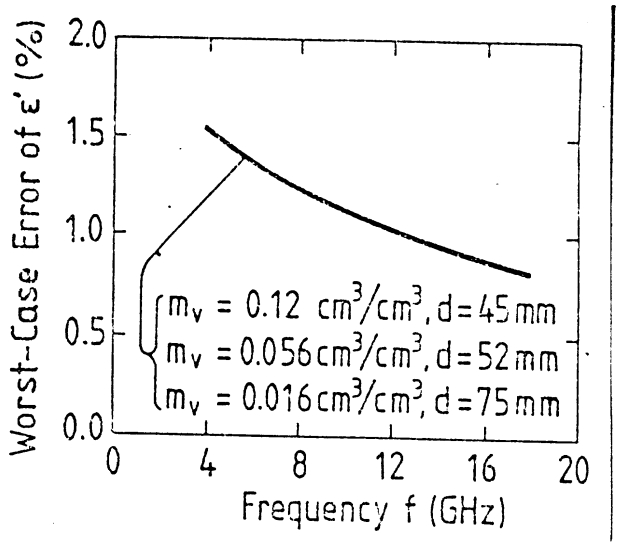

(a)

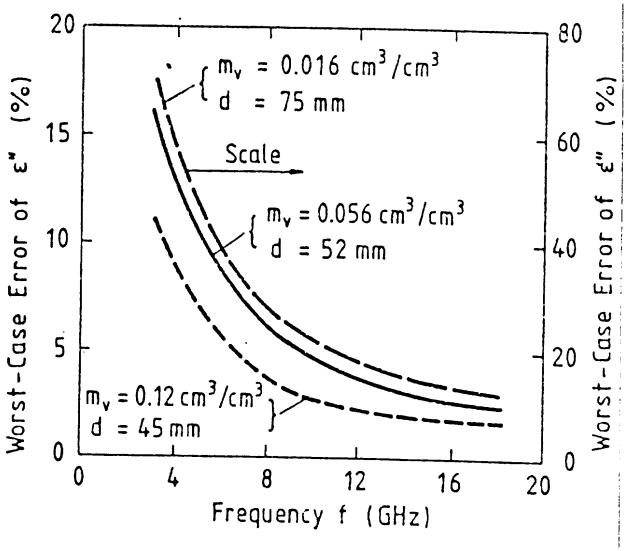

(b)

Fig. 3. Calculated worst-case error bounds for (a) measured snow permittivity and (b) measured loss factor as a function of frequency, with volumetric water content and sample thickness as

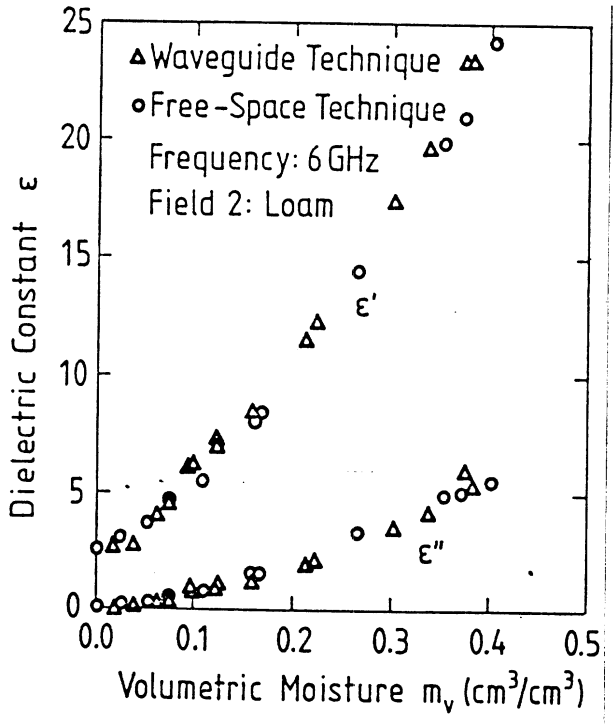

Fig. 4. Comparison of the free-space transmission system against a waveguide transmission system at 6 GHz.

2.3 Sample Preparation

The snow samples were acquired from the open area near the facilties of the Remote Sensing Laboratory of the University of Kansas, Lawrence, Kansas. The samples were acquired from different depths in the snow cover, including the bottom and the top layers. Extreme care was taken not to disturb the structure of the samples. First, the extra snow around a potential sample was removed and the sample holder was placed upside down on the top of the sample. Then the sample was properly cut and its surface was smoothed by cutting the extra snow out with a slab.

After completing the microwave dielectric measurements using the 3- to 18-GHz and the 37-GHz free-space system, the sample holder containing the sample of snow was weighted and the thickness of the sample was measured. The sample temperature was measured using a temperature probe and a digital multimeter. The freezing calorimeter method was used to measure the snow liquid water content. Immediately after the snow liquid water content was measured, snow crystal parameters were observed using a microscope with a fiber optic light source to minimize heating effects on the snow sample. The pH level of the snow samples was examined with each new snowfall. A small sample of snow was allowed using a pH meter.

In order to obtain the density of dry snow from the measured density of wet snow sample, the following expression, used by Ambach and Denoth [23], was used in this study:

$$\rho_{ds} = \frac{\rho_{ws} - m_v}{1.0 - m_v} \qquad (6)$$

where ρ_{ds} is the density of dry snow in g/cm^3, ρ_{ws} is the density of wet snow in g/cm^3, and m_v is the volume fraction of liquid water (volumetric water content) within the snow sample.

During the 1982 experiment the snow samples were not insulated at their upper surface, and therefore the snow liquid water content varied with time during the measurement. In order to find the actual water content as a function of time, the first and the last measurement of each sample was made at 18 GHz. This allowed the calorimetrically measured water content to be properly corrected. In 1983 the samples were insulated with styrofoam and no corrections were needed.

3.0 EXPERIMENTAL DATA

A comprehensive data base of the snow complex dielectric constant between 3 GHz and 37 GHz was established in 1982 and 1983. In 1982, the measurements were conducted at 9 equally spaced frequencies between 4 GHz and 18 GHz. In 1983, two frequencies were added, resulting in a frequency range of 3 to 37 GHz.

The data base of the snow dielectric measurements consists of 995 data points, 584 of which are for wet snow and 411 are for dry snow. The number of snow samples measured at each frequency between 4 GHz and 18 GHz (using 2-GHz intervals) is about 110, whereas 63 samples were measured at 3 GHz and at 37 GHz. The snow samples had densities ranging from 0.09 g/cm^3 to 0.42 g/cm^3 and liquid water contents ranging between 0% and 12.3% by volume. The snow particle size varied between 0.5 mm and 1.0 mm and the pH level ranged from 5.6 to 6.5. The samples had temperatures ranging from -5°C to 0°C. All snow samples were of fairly new snow. Two examples of the experimental data are given in Figures 5 and 6. The results of the 1983 measurements agree well with those obtained in 1982. The scatter in ε''_{wc} is larger at 4 GHz than

measured at all frequencies. Because the sample loss is lower at low frequencies than at high frequencies, the measurement of ε''_{ws} is less accurate at 4 GHz than at 18 GHz.

In addition, the loss of several dry snow types was measured at 37 GHz where volume scattering is the dominant loss mechanism. Different thicknesses for each snow type were used in order to increase the accuracy. Some samples were stored for one year in a freezer before the measurement. The density of the samples ranged from 0.32 g/cm^3 (new snow) to 0.43 g/cm^3 (refrozen snow) and the grain size from 1.0 mm to 1.5 mm, correspondingly. The temperature of the samples was -15°C.

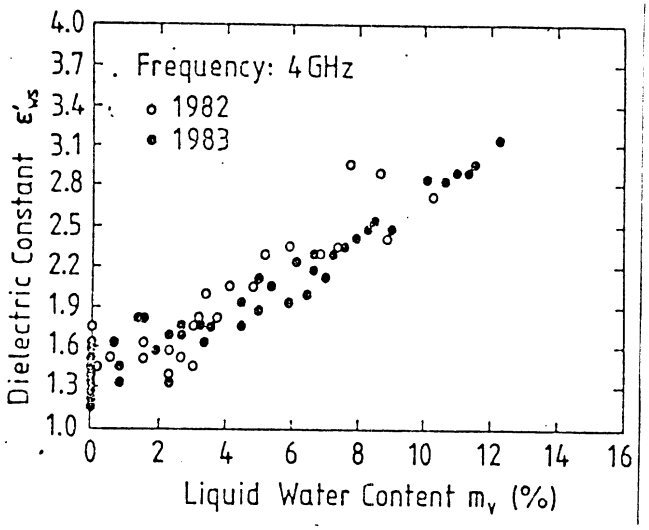

(a)

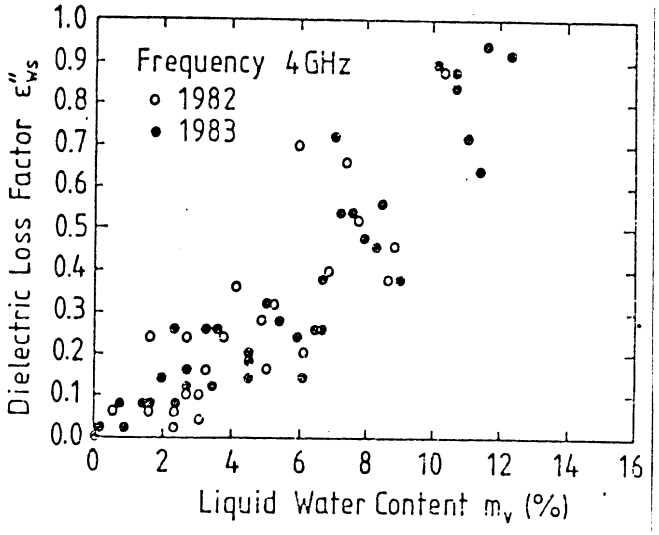

(b)

Figure 5. Comparison of the 1982 and 1983 measurements for (a) the dielectric constant and (b) the loss factor of snow at 4 GHz.

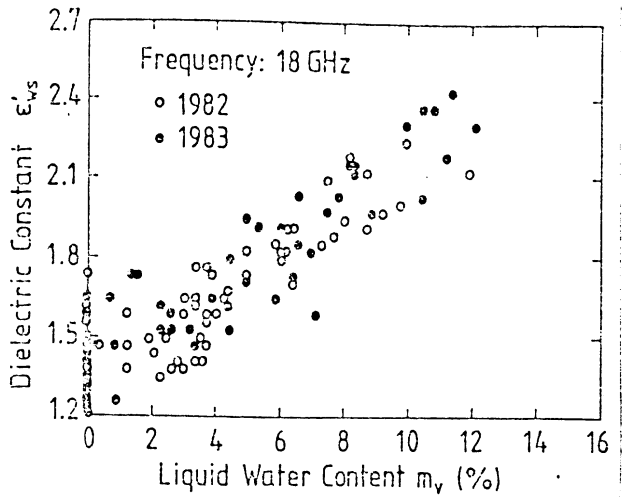

(a)

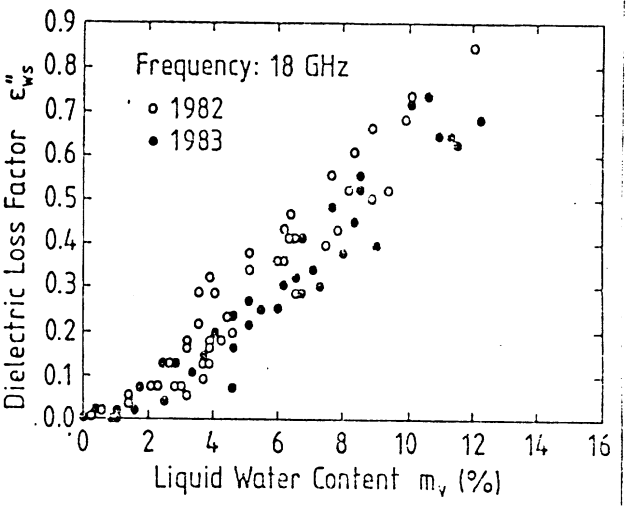

(b)

Figure 6. Comparison of the 1982 and 1983 measurements for (a) the dielectric constant and (b) the loss factor of snow at 18 GHz.

4.0 DIELECTRIC MODELS

The experimental data were used to develop and evaluate several theoretical and empirical snow dielectric models. The evaluation of the models was performed using the residual sum of squares, given by

$$RSS = \sum_{i=1}^{n} [\varepsilon_i(obs) - \varepsilon_i(pred)]^2, \qquad (7)$$

where $\varepsilon_i(obs)$ is the measured value, $\varepsilon_i(pred)$ is the estimate and n is the number of data points. Equation (7) was used separately for ε' and ε''.

The rms error for ε' is

$$e'_{rms} = [RSS/n]^{\frac{1}{2}} \qquad (8)$$

and a similar expression applies to ε''.

The square of the correlation coefficient, r^2, measures the proportion of the total variation about the mean value explained by the regression.

As a third criterion, linear regressions of the form

$$\varepsilon'(\text{obs}) = \alpha'\varepsilon'(\text{pred}) + \beta' \qquad (9)$$

$$\varepsilon''(\text{obs}) = \alpha''\varepsilon''(\text{pred}) + \beta'' \qquad (10)$$

were used to evaluate the models. A perfect model is one for which $\alpha' = \alpha'' = 1$ and $\beta' = \beta'' = 0$, and for which the linear regression coeffients for ε'_{ws} and ε''_{ws} are close to unity in magnitude.

4.1 Dry Snow

Dry snow is a mixture of ice and air. The permittivity of ice is independent of temperature and frequency at microwave frequencies [24]. This causes the permittivity of dry snow ε'_{ds} to be also independent of temperature and frequency. The acquired data for ε'_{ds} in the 3- to 37-GHz range, shown in Figure 7, were found to follow a linear density dependence, given by

$$\varepsilon'_{ds} = 1.8317\ \rho_{ds} \quad ;\ 0.09 \lesssim \rho_{ds} \lesssim 0.40\ \text{g/cm}^3. \qquad (11)$$

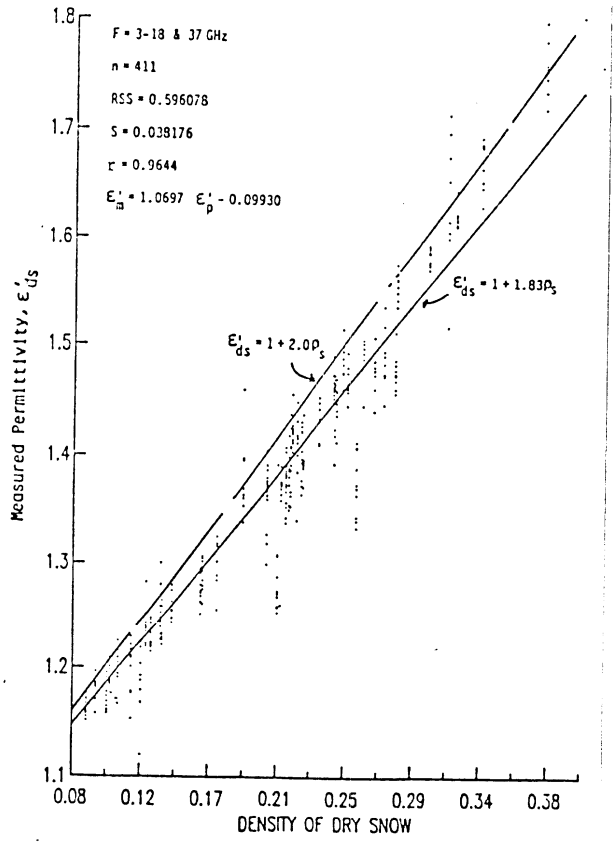

Figure 7. Measured dielectric constant for dry snow as a function of density between 3 and 37 GHz.

The estimate of the rms error between the measured values and those predicted by Equation (11) is 0.038. However, Equation (11) tends to overestimate the values of ε'_{ds} for low snow densities and underestimate them for high snow densities. By combining the present data with previous experimental values [11,15,25], two expressions have been derived for ε'_{ds}:

$$\varepsilon'_{ds} = 1 + 1.9\ \rho_{ds};\ \rho_{ds} \lesssim 0.5\ \text{g/cm}^3 \qquad (12a)$$

$$\varepsilon'_{ds} = 0.51 + 2.88\ \rho_{ds}\ ;\ \rho_{ds} \gtrsim 0.5\ \text{g/cm}^3. \qquad (12b)$$

Expressions similar to Equation (11) have been reported in the literature for frequencies below 13 GHz with slightly larger values for the coefficient of ρ_{ds} [23,26]. The larger values are due to the higher range of density of the tested snow samples. In this paper, Equation (11) will be used to describe the dependence of ε'_{ds} on snow density.

The imaginary part (or loss factor) of the dielectric constant of dry snow, ε''_{ds}, is of the order of 10^{-3} in the microwave region, and therefore difficult to measure with a good degree of accuracy. The cavity technique is needed for measuring the dielectric properties of very low loss materials. The measurements of ε''_{ds} made with the free-space transmission system are not accurate enough to use for model evaluations. From the theoretical Polder and Van Santen mixing model [27], the following formula may be obtained by assuming the ice particles to be spherical

$$\varepsilon''_{ds} = \frac{0.34\ v_i \varepsilon''_i}{(1 - 0.417\ v_i)^2}, \qquad (13)$$

where $v_i = \rho_{ds}/\rho_i$ is the ice volume fraction, $\rho_i = 0.916\ \text{g/cm}^3$ is the density of ice, and ε''_i is the loss factor of ice. Figure 8 shows that $\varepsilon''_{ds}/\varepsilon''_i$ from Equation (13) agrees well with Cummings' data for dry snow over a wide snow density range. The dependence of ε''_i on frequency and temperature has been examined by Nyfors [15], and by Stiles and Ulaby [28].

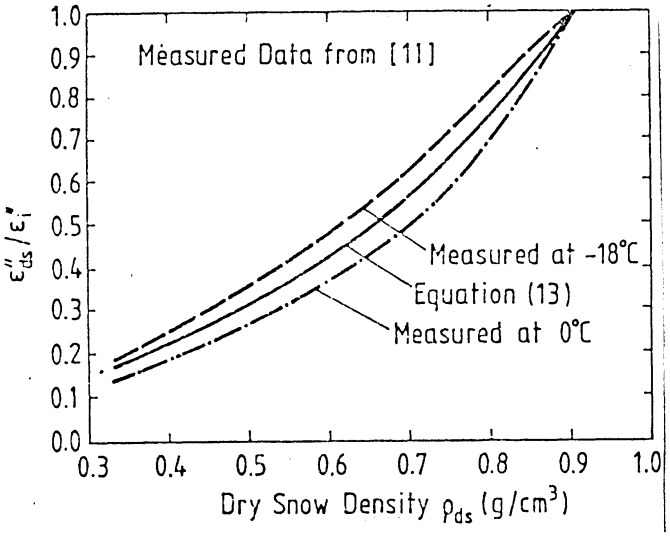

Figure 8. Comparison of Equation (13) with Cumming's experimental data [11] for the loss factor of dry snow relative to that of ice.

4.2 Wet Snow

Six dielectric mixing models were considered including (a) the two-phase Polder and Van Santen Model [27] (dry snow and water mixture), (b) the three-phase Polder and Van Santen model (ice, air, and water), (c) the confocal ellipsoidal model [29], (d) the refractive model [31], (e) an empirical model based on Linlor's formulation [14], and (f) a Debye-like semi-empirical model described below. Of these, only models (a), (b), and (f) provided results in good agreement with experimental observations.

In the theoretical models, wet snow is assumed to consist of either dry snow (with $\varepsilon_{ds} = \varepsilon'_{ds} - j\varepsilon''_{ds}$) and water (with $\varepsilon_w = \varepsilon'_w - \varepsilon''_w$), or of air (with $\varepsilon_a = 1$), ice (with $\varepsilon_i = \varepsilon'_i - j\varepsilon''_i$), and water. For dry snow, ε'_{ds} is calculated from Equation (11) and ε''_{ds} is set equal to 0.002 [28]; for water, ε_w is calculated from the Debye equation [3]; and for ice, $\varepsilon'_i = 3.15$ [24] and ε''_i is calculated from [15].

Two-Phase Polder and Van Santen Model

The complex dielectric constant of wet snow, $\varepsilon_{ws} = \varepsilon'_{ws} - j\varepsilon''_{ws}$, is assumed to be a mixture of dry snow as host and liquid water as inclusions. The water particles are randomly distributed and randomly oriented ellipsoids with depolarization factors A_{w1}, A_{w2}, and A_{w3}. The mixing formula [28] is given by

$$\varepsilon_{ws} = \varepsilon_{ds} + \frac{m_v\, \varepsilon_{ws}}{3} (\varepsilon_w - \varepsilon_{ds}) \sum_{j=1}^{n} [\varepsilon_{ws} + (\varepsilon_w - \varepsilon_{ws})\, A_{wj}]^{-1}, \quad (14)$$

where m_v is the liquid water content (volume fraction of water).

In previous modeling efforts of wet snow using the two-phase Polder and Van Santen mixing model, the water inclusions have been assumed to be symmetrical in shape, that is $A_{w1} = A_{w2}$, and $A_{w3} = 1 - 2\,A_{w1}$ [18]. On the other hand, there is some evidence that the shape of water inclusions may vary as a function of water content. Ambach and Denoth [18] fitted their experimental data for ε'_{ws} (below 1 GHz) using the symmetrical approach. They observed the optimum value of A_{w1} to vary between 0.01 and 0.08, generally increasing with increasing water content.

Three different approaches were taken in the present investigation when applying the two-phase Polder and Van Santen mixing model: (a) the water inclusions were assumed to be symmetrical in shape ($A_{w1} = A_{w2}$, $A_{w3} = 1 - 2\,A_{w1}$) and their shape to be independent of snow water content, (b) the water inclusions were assumed to be nonsymmetrical in shape ($A_{w1} \neq A_{w2} \neq A_{w3}$), and their shape to be independent of snow water content, and (c) the water inclusions were assumed to be nonsymmetrical in shape, and their shape to depend on snow water content. In each case, optimum values for A_{wi} were sought by minimizing the error between the values of ε_{ws} as calculated from Equation (14) and those obtained experimentally.

Table 2 shows the results from the optimization processes. The symmetrical approach gave $A_{w1} = 0.074$ when the optimization was performed using ε''_{ws} data. However, the corresponding value using ε'_{ws} data was $A_{w1} = 0.155$. The fact that different depolarization factors are needed to describe the behavior of ε'_{ws} and ε''_{ws} renders the symmetrical approach unacceptable. This suggests that the water inclusions in snow do not accommodate themselves in a symmetrical shape.

The second approach, in which the water inclusions were assumed to be nonsymmetrical in shape and to conserve their shape independent of snow water content, gave $A_{w1} = 0.067$ and $A_{w2} = 0.251$

when the optimization was performed using ε''_{ws} data. The superiority of the nonsymmetrical approach compared to the symmetrical one is indicated by the fact that the same set A_{wi} (optimized using ε''_{ws} data) gives a reasonably good fit to ε'_{ws} data as well.

Finally, A_{w1}, A_{w2}, and A_{w3} were optimized separately as a function of water content using ε''_{ws} data. Each water content category was Δm_v = 1% in range, that is $0.0 \leq m_{v1} < 1.0 \leq m_{v2} < 2.0\%$ etc., and the last region $11.0 \leq m_{v12} < 12.5\%$. The optimized depolarization factors are shown in Figure 9 as a function of liquid water content. According to the results, the water inclusions in snow appear needle-like in shape (A_{w1} = 0.0, $A_{w2} = A_{w3}$ = 0.5 for needles) for liquid water contents below m_v = 3%. However, they change into disc-like shapes for $m_v \geq 3\%$ ($A_{w1} = A_{w2}$ = 0.0, A_{w3} = 1.0 for discs). This change in shape for the water inclusions appears to be that of the transition from the pendular regime to the funicular regime.

The transition value is lower than that calculated by Colbeck [17]; however, the low snow density in the present study could be expected to decrease the transition value.

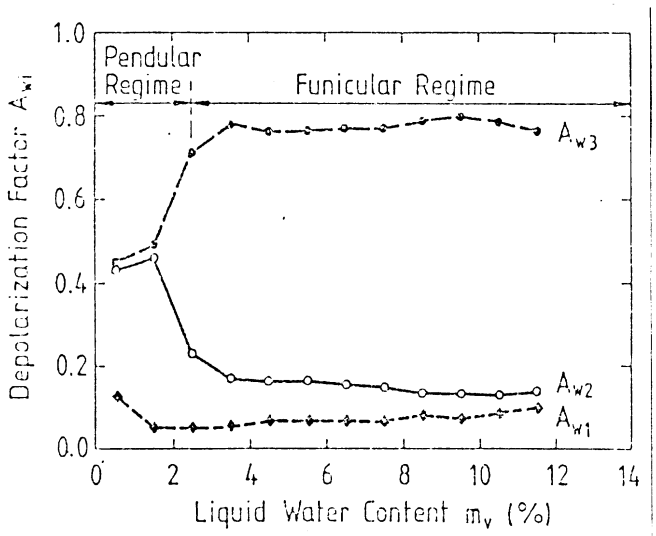

Figure 9. Depolarization factors A_{w1}, A_{w2}, and A_{w3} for water inclusions in snow, optimized by fitting the two-phase Polder and Van Santen model to the measured values of ε''_{ws}.

The two-phase Polder and Van Santen model with nonsymmetrical water inclusions (and whose shape depends on the snow water content) is found to be in excellent agreement with the measured ε''_{ws} data as shown in Table 2. The depolarization factors optimized previously, using the measured values of ε''_{ws}, as a function of m_v, can be used in the two-phase Polder and Van Santen mixing model to estimate the values of ε'_{ws}. Table 2 shows the statistics of the predicted ε'_{ws} values as compared to the measured values. The model works well at all frequencies.

Three-Phase Polder and Van Santen Model

Instead of treating wet snow as a two-phase mixture of dry snow and liquid water, the three-phase mixing model treats it as a mixture of air (as host), ice, and liquid water. The expression for ε_{ws} is fundamentally similar to that given in Equation (14) except that it contains two summations: one over the depolarization factors of the ice inclusions (assumed to be spherical) and another over the depolarization factors of water [28]:

$$\varepsilon_{ws} = 1 + \frac{1}{3}\varepsilon_{ws} v_i(\varepsilon_i - 1) \sum_{j=1}^{3} [\varepsilon_{ws} + (\varepsilon_i - \varepsilon_{ws})A_{ij}]^{-1} + \frac{1}{3}\varepsilon_{ws} m_v(\varepsilon_w - 1) \sum_{j=1}^{3} [\varepsilon_{ws} + (\varepsilon_w - \varepsilon_{ws})A_{wj}]^{-1}. \quad (15)$$

In Equation (15), m_v is the volume fraction of water (= liquid water content), and A_{wj} and A_{ij} are the depolarization factors of the water and ice inclusions, respectively, with A_{ij} = 1/3. Again, the three different approaches concerning the depolarization factors of the water inclusions were taken.

Table 3 shows the results from the optimization processes. The symmetrical approach gave A_{w1} = 0.084 when the values were optimized using ε''_{ws} data, and A_{w1} = 0.189 when the values were optimized using ε'_{ws} data. The results are close to those obtained using the corresponding two-phase Polder and Van Santen model and they suggest again that the water inclusions in snow are not symmetrical.

Using the nonsymmetrical approach, with the shape of the water inclusions independent of the snow water content, gives A_{w1} = 0.047 and A_{w2} = 0.372. The best agreement with the measured ε''_{ws} and

ε'_{ws} data is again obtained by assuming the water inclusions to be nonsymmetrical in shape and their shape to depend on the snow water content. The optimized values of A_{wi}, using ε''_{ws} data, are shown in Figure 10 as a function of water content. Although there is more scatter in A_{wi} than in the corresponding values using the two-phase Polder and Van Santen model, the average values of A_{wi} from the two models are close to each other.

The three-phase Polder and Van Santen model is capable of predicting both ε'_{ws} and ε''_{ws} reasonably well. The transition from the pendular regime to the funicular regime takes place again around m_v = 3%.

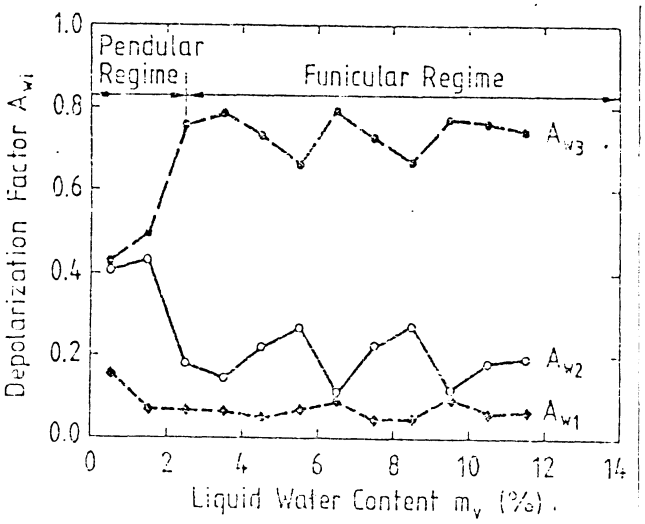

Figure 10. Depolarization factors A_{w1}, A_{w2}, and A_{w3} for water inclusions in snow, optimized by fitting the three-phase Polder and Van Santen model to the measured values of ε''_{ws}.

Debye-Like Model

The dieletric constant of dry snow is of the order of $\varepsilon_{ds} \cong 1.6 - j10^{-3}$. The water inclusions have an ε'_w that is about 40 times larger than ε'_{ds}. Hence, even when the liquid water content is of the order of only 1 percent by volume, the spectral behavior of the wet snow mixture is likely to be dominated by the dispersion behavior of water. This argument led to the testing of the following semi-empirical model:

$$\varepsilon'_{ws} = A + \frac{B\, m_v^{\,x}}{1 + (f/f_0)^2} \tag{16}$$

$$\varepsilon''_{ws} = \frac{C\, f\, m_v^{\,x}}{1 + (f/f_0)^2} \tag{17}$$

where f_0 is the relaxation frequency, f is frequency, and A, B, C, and x are constants to be determined by fitting the model to the measured data in the 3- to 37-GHz range. Such an approach gives

$$A = 1.0 + 1.83\, \rho_{ds} + 0.02\, m_v^{\,1.015} \tag{18a}$$

$$B = 0.073 \tag{18b}$$

$$C = 0.008 \tag{18c}$$

$$x = 1.31 \tag{18d}$$

$$f_0 = 9.07 \text{ GHz}. \tag{18e}$$

The value of f_0 is slightly higher than the relaxation frequency of water at 0°C, f_{ow} = 8.8 GHz [3]. This is in agreement with the results of previous studies concerning heterogeneous mixtures containing water. De Loor has found out both theoretically and experimentally that the relaxation frequency of such mixtures is always equal to or higher than that of the relaxing component [30]. In addition, he concluded that the closer the relaxation frequency of the mixture is to the relaxation frequency of the inclusions, the greater is the departure of the shape of the inclusions from spherical (approaching discs or needles). Therefore, the optimized nonsymmetrical values for A_{wi} in the Polder and Van Santen models in the previous sections are in agreement with the value of the relaxation frequency in Equation (18e).

In order to increase the accuracy of the Debye-like model, polynomial expressions relating the values of α', α'', β' and β'' in Equations (9) and (10) to frequency were developed:

$$\alpha' = 0.7816 + 0.0311\, f - 0.5810 \times 10^{-3} f^2 \tag{19a}$$

$$\beta' = 0.3094 - 0.0450\, f + 0.8696 \times 10^{-3} f^2 \tag{19b}$$

$$\alpha'' = 0.9741 - 0.3894 \times 10^{-2} f + 0.39099 \times 10^{-3} f^2 \tag{19c}$$

$$\beta'' = 0.0. \tag{19d}$$

In Equation (19), f is the frequency in GHz. In this paper, the model including Equations (17) to (20 is called the modified Debye-like model.

5.0 EVALUATION OF THE DIELECTRIC MODELS

In order to compare the calculated contribution of water to the measured values, an incremental permittivity value, $\Delta\varepsilon'_{WS}$, that is independent of density is used:

$$\Delta\varepsilon'_{WS} = \varepsilon'_{WS} - \varepsilon'_{ds} = \varepsilon'_{WS} - 1.0 - 1.8317\,\rho_{ds}. \quad (20)$$

$\Delta\varepsilon'_{WS}$ shows the contribution of liquid water in snow. For ε''_{WS} no incremental value is needed because liquid water dominates the loss factor.

Figure 11 shows the measured permittivity and dielectric loss factor at 6 GHz as a function of liquid water content. The solid curves were calculated using the Debye-like model. As indicated by these figures, the fit is quite good.

Similar fits were also obtained with the Polder and Van Santen models. The difference in behavior between the Debye-like model and the Polder and Van Santen models is significant only at frequencies above 15 GHz; Figure 12 provides a comparison of the two models with the data at 37 GHz.

The overall fit of the two-phase Polder and Van Santen model to the data is shown in the form of the scatter plots in Figure 13.

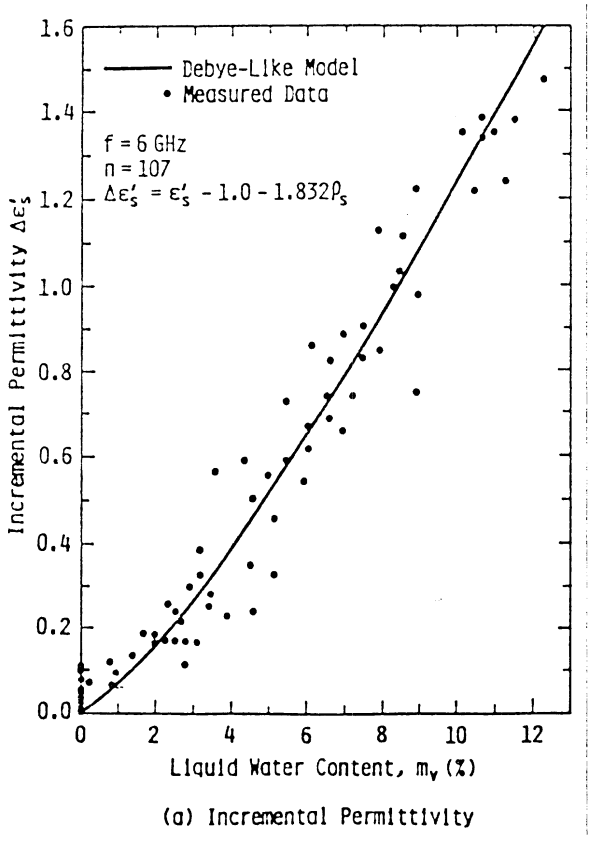

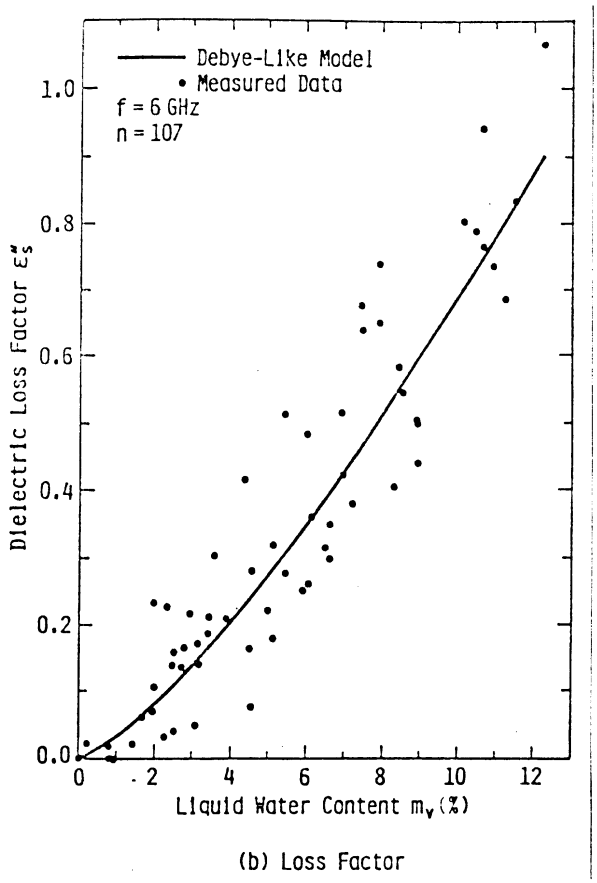

Figure 11. Comparison of model predictions with measured values of $\Delta\varepsilon'_{ws}$ at 6 GHz, 12 GHz, and 37 GHz.

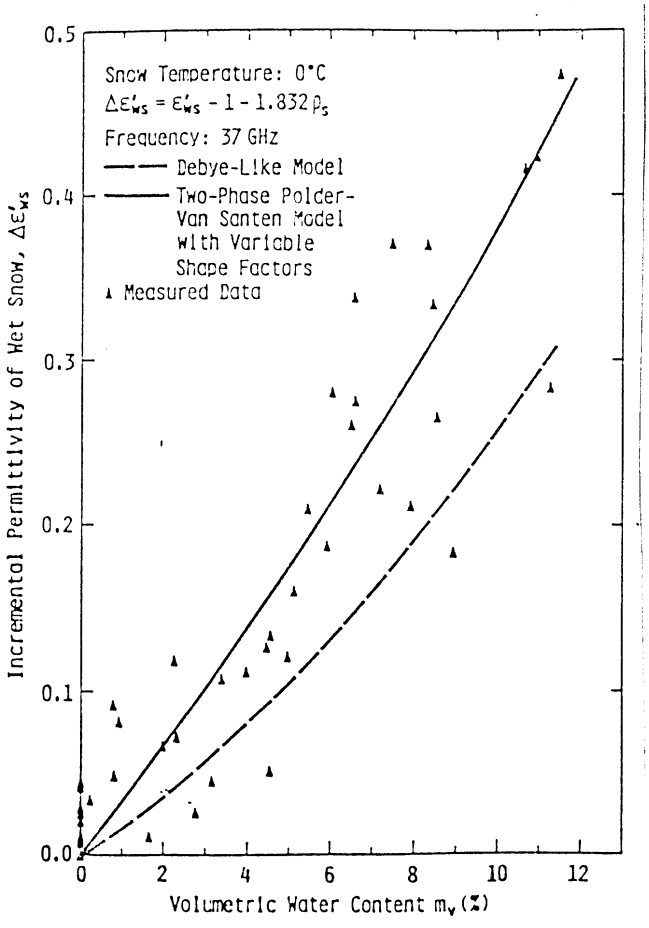

(a)

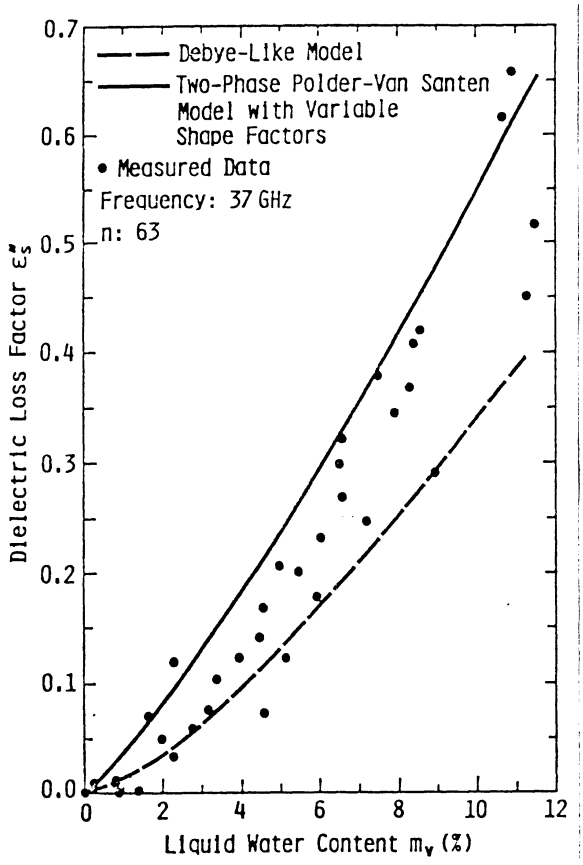

(b)

Figure 12. Comparison of model predictions with measured values of ε''_{ws} at 6 GHz, 12 GHz, and 37 GHz.

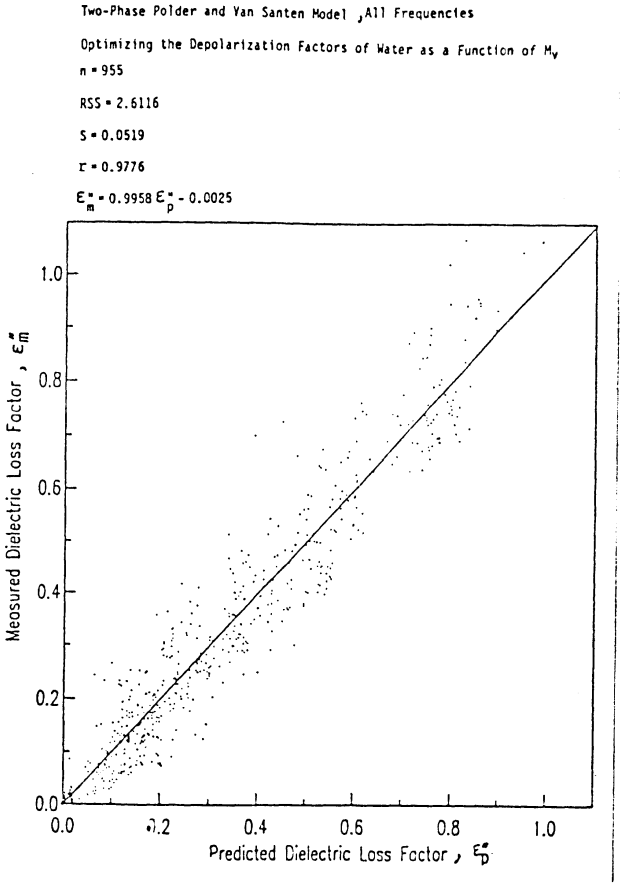

(b)

Figure 13. Comparison of the two-phase Polder and Van Santen model predictions with experimental data for (a) ε'_{ws} and (b) ε''_{ws}.

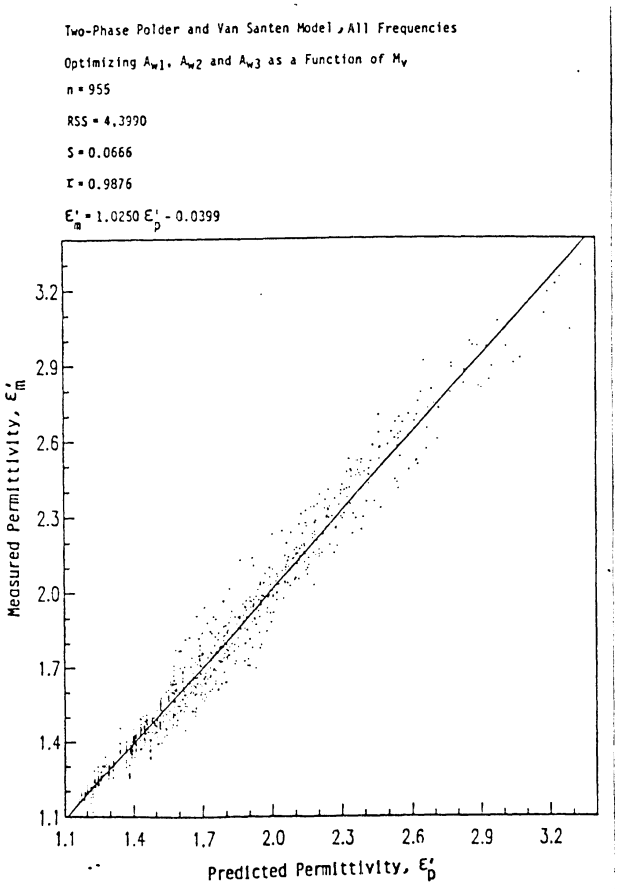

(a)

A quantitative comparison of the models is provided in Table 4 for ε'_{ws} and in Table 5 for ε''_{ws}. It is obvious that the Polder and Van Santen models provide the best overall agreement with the measured ε_{ws} data. The confocal ellipsoidal model gives a poor fit to the experimental data and the Linlor-like model gives a good fit for ε'_{ws} but does not have an expression for ε''_{ws}.

6.0 DISPERSION BEHAVIOR OF WET SNOW

Figures 14 to 16 show the effect of liquid water content on the dielectric behavior of wet snow between 3 GHz and 37 GHz. The results are shown for a dry snow density ρ_{ds} = 0.24 g/cm^3, which was the average observed value in this study. The values of ε'_{ws} and ε''_{ws} were calculated using the modified Debye-like equation discussed in Section 4.2. As shown by Figures 14 to 16, ε''_{ws} has its maximum value at 9.0 GHz. This agrees with the relaxation frequency of water at 0°C. The sharp increase in ε''_{ws} between 3 GHz and 6 GHz is due to the large difference in the values of ε''_w for

water between 3 GHz and 6 GHz, as illustrated in Figure 17.

The attenuation constant of wet snow increases practically linearly with frequency up to 15 GHz. Between 18 GHz and 37 GHz, the average slope is slightly smaller. The penetration depth decreases with increasing frequency and increasing liquid water content, as illustrated in Figure 18. For m_v = 5%, the penetration depth is about 20 cm at 4 GHz, 3 cm at 10 GHz and less than 1 cm at 37 GHz. The effect of volume scattering is included in the results shown in Figure 18.

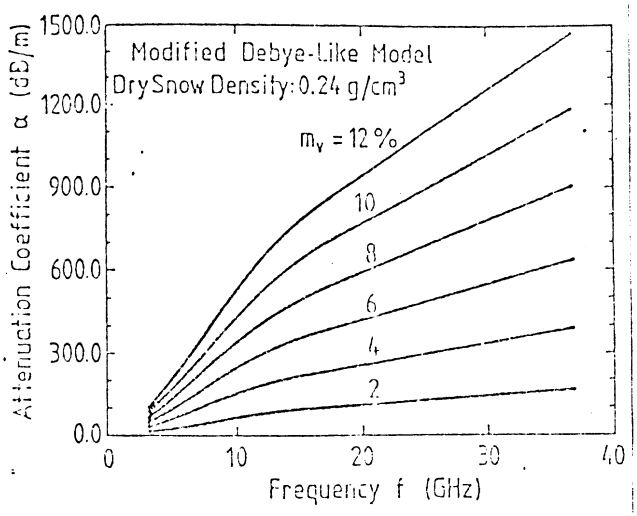

Figure 16. Attenuation coefficient of snow, predicted by the modified Debye-like model, as a function of frequency with liquid water content as a parameter.

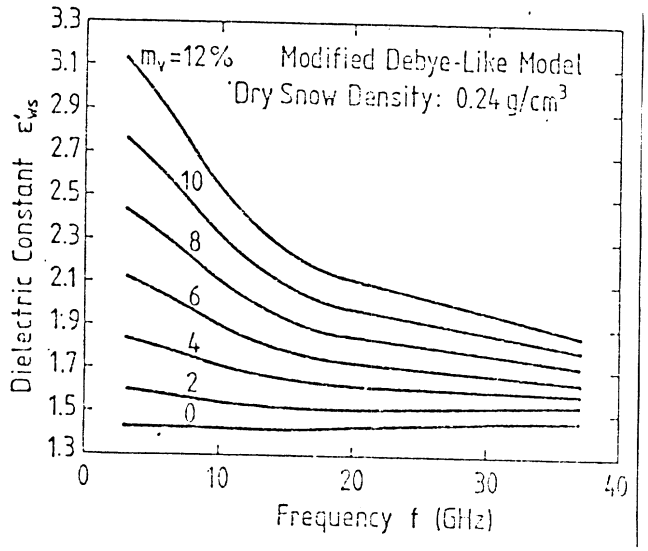

Figure 14. Dielectric constant of snow, predicted by the modified Debye-like modek, as a function of frequency with liquid water content as a parameter.

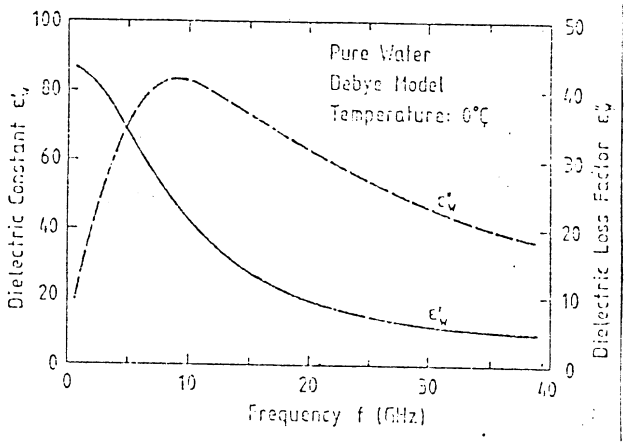

Figure 17. Dielectric behavior of water as a function of frequency at 0°C.

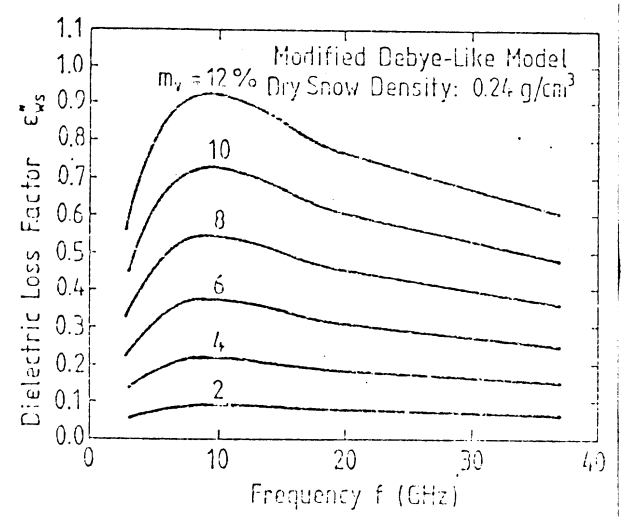

Figure 15. Loss factor of snow, predicted by the modified Debye-like model, as a function of frequency with liquid water content as a parameter.

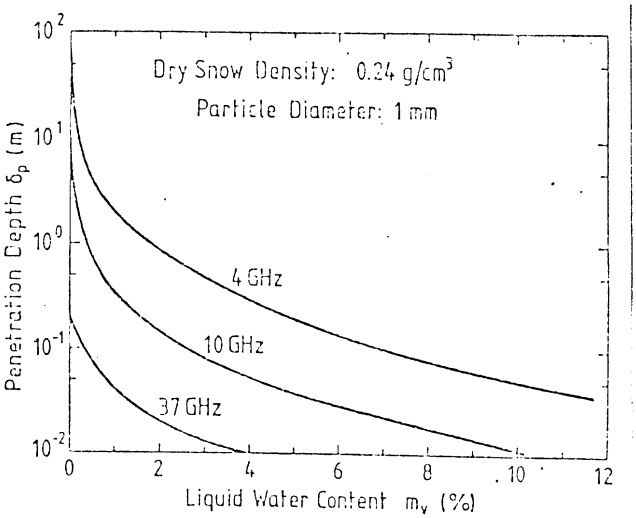

Figure 18. Calculated penetration depth as a function of liquid water content at 4 GHz, 10 GHz, and 37 GHz.

Simple numerical expressions relating $\Delta\varepsilon'_{ws}$ and ε''_{ws} to the water content of snow have been developed in recent studies to calibrate snow wetness sensors that operate at frequencies below 1 GHz [18,26]. Expressions of the form

$$\Delta\varepsilon'_{ws} = k_1 m_v \quad (21a)$$

$$\varepsilon''_{ws} = k_2 m_v \quad (21b)$$

have been developed for the 3- to 37-GHz range using the results from the modified Debye-like model in Figures 14 and 15. Average values for the coefficients k_1 and k_2 in the 0- to 12.3% volumetric water content range are listed in Table 6. Since the water content dependence of $\Delta\varepsilon'_{ws}$ and ε''_{ws} is slightly nonlinear, the values for k_1 and k_2 in Table 6 tend to overestimate both quantities at small water contents and underestimate them at high water contents.

7.0 VOLUME SCATTERING BY SNOW

The dielectric loss factor of dry snow, ε''_{ds}, is of the order of 10^{-3} at microwave frequencies. Therefore, ε''_{ds} cannot be measured accurately with a free-space transmission system; however, the scattering loss can be measured at 37 GHz.

The total loss of a snow medium is given by the extinction coefficient κ_e:

$$\kappa_e = \kappa_a + \kappa_s. \quad (22)$$

In Equation (22), κ_a is the power absorption coefficient ($\kappa_a = 2\alpha$) and κ_s is the corresponding scattering coefficient.

With increasing frequency and snow particle size, volume scattering increases rapidly and finally replaces dielectric loss as the dominant loss mechanism. As illustrated in Figure 19, this occurs at a frequency of 14 GHz for snow with a particle diameter of 1 mm. The results shown in Figure 19 were obtained using the Mie scattering theory.

Snow density plays an important role in volume scattering loss. This is because the density of dry snow determines the number of ice particles per unit volume of snow, and therefore the number of scattering particles. Figure 20 shows plots of κ_a, κ_s, and κ_e as a function of snow density at 37 GHz, for snow with particles of 1 mm in diameter. The variation of κ_a, κ_s, and κ_e is linear with snow density.

The total loss (mainly scattering loss) was measured for four snow types at 37 GHz. The properties of the snow types are listed in Table 7. For each snow type, samples with several thicknesses were used. As illustrated in Figure 21, all the samples that had undergone a melt-refreeze process show scattering losses that are practically the same. Only the newly fallen snow shows a considerably smaller loss. It is therefore concluded that a distinction can be seen in the scattering loss between newly fallen snow and refrozen snow that has undergone the melt-refreeze process. Additionally, the influence of mechanically breaking the continuous ice structure seems to be fairly small.

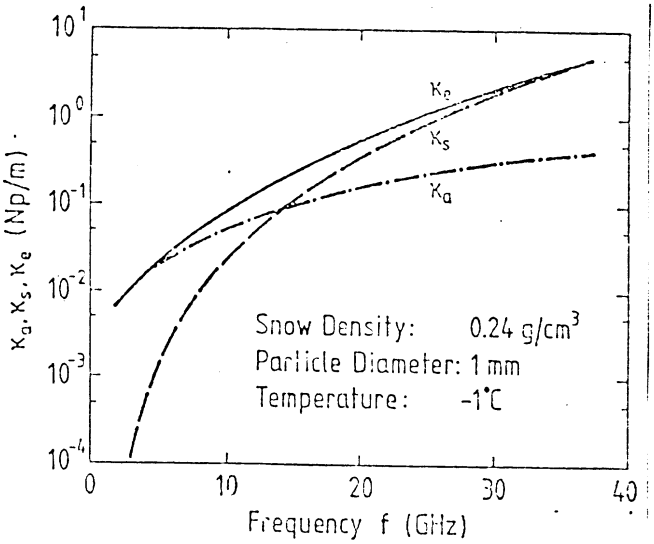

Figure 19. Calculated extinction coefficient κ_e, scattering coefficient κ_s, and absorption coefficient κ_a for dry snow as a function of frequency.

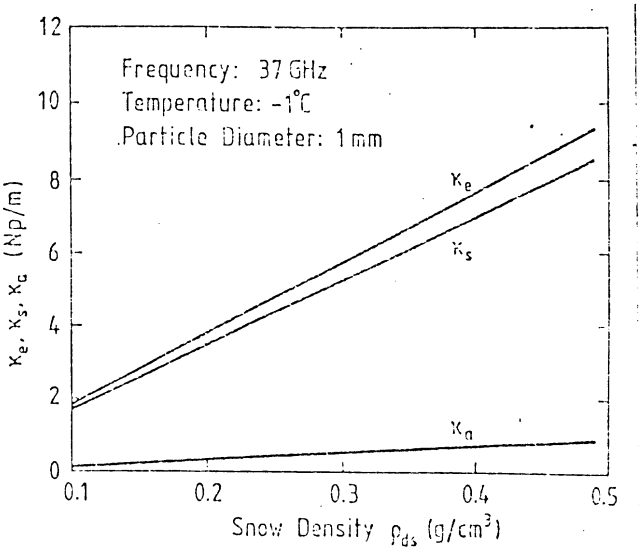

Figure 20. Calculated extinction coefficient κ_e, scattering coefficient κ_s, and absorption coefficient κ_a as a function of dry snow density at 37 GHz.

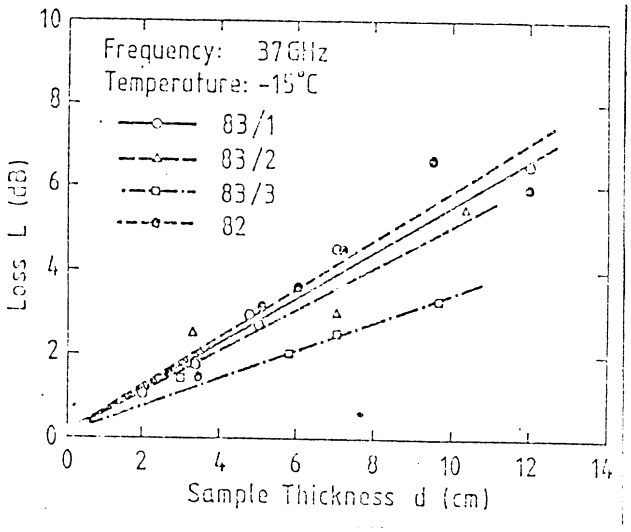

Figure 21. Measured total loss for four dry snow types (Table 7) at 37 GHz.

Table 8 shows a comparison between the values of κ_e calculated from the Mie scattering expressions and the measured values. In general, the calculated values are larger. The difference may be partly due to errors in determining the average snow particle size. The estimates were obtained using a microscope.

8.0 CONCLUSIONS

The following conclusions can be made from this study of the dielectric behavior of snow in the 3- to 37-GHz range:

(a) The dielectric constant of dry snow increases practically linearly with increasing snow density.

(b) The dispersion behavior of water determines the spectral behavior of wet snow. Similar to liquid water, the relaxation frequency of wet snow is approximately 9.0 GHz.

(c) Volume scattering is the dominant loss mechanism in dry snow above 14 GHz for a snow particle size of 1 mm or larger. Undergoing the melt-refreeze cycle increases the extinction coefficient of dry snow at 37 GHz. The scattering loss decreases drastically with increasing liquid water content, becoming negligible for m_v values above 1%.

(d) The modified Debye-like model is the best of the developed empirical models to describe the dielectric behavior of snow as a function of its physical parameters and frequency.

(e) If nonsymmetry is assumed for the depolarization factors of the water inclusions, the two-phase and three-phase Polder and Van Santen models can adequately describe the dielectric behavior of snow.

(f) The water inclusions in the snow were found to be needle-like in shape as the water appears in the snow. A transition in their shape occurs around m_v = 3% into a disc-like shape. These results were obtained by optimizing the shape of the water inclusions to fit the two-phase and three-phase Polder and Van Santen models to the measured values of ε''_{ws}.

REFERENCES

1. Gray, D. M., and D. H. Male (eds.), 1981, Handbook of Snow; Principles Processes, Management and Use, Toronto, Oxford, New York; Pergamon Press.

2. Colbeck, S. C., 1982, The Geometry and Permittivity of Snow at High Frequencies, J. Appl. Phys., Vol. 53, No. 6, pp. 4495-4500.

3. Ulaby, F. T., R. K. Moore, and A. K. Fung, 1982-1985, Microwave Remote Sensing - Active and Passive, Vol. I and III, Addison-Wesley Pub. Co., Inc., Reading, MA.

4. Stiles, W. H., and F. T. Ulaby, 1980, Microwave Remote Sensing of Snowpacks, NASA Report 3263, Contract NAS 5-23777, Goddard Space Flight Center, Greenbelt, MD.

5. Ulaby, F. T., and W. H. Stiles, 1980, The Active and Passive Microwave Response to Snow Parameters, Part II: Water Equivalent of Dry Snow, J. Geophys. Res., Vol. 83, No. C2, pp. 1045-1049.

6. Hofer, R., and C. Mätzler, 1980, Investigations on Snow Parameters by Radiometry in the 3- to 60-mm Wavelength Region, J. Geophys. Res., Vol. 85, No. C1, pp. 453-460.

7. Tiuri, M., 1982, Theoretical and Experimental Studies of Microwave Emission Signatures of Snow, IEEE Trans. Geosci. and Rem. Sens., Vol. GE-20, pp. 51-57.

8. Mätzler, C., E. Schanda, and W. Good, 1982, Towards the Definition of Optimum Sensor Specification for Microwave Remote Sensing of Snow,

IEEE Trans. Geosci. and Rem. Sens., Vol. GE-20, No. 1, pp. 57-66.

9. Künzi, K., S. Patil, and H. Rott, 1982, Snow-Cover Parameters Retrieved from Nimbus-7 Scanning Multichannel Microwave Radiometer (SMMR) Data, IEEE Trans. Geosci. and Rem. Sens., Vol. GE-20, pp. 452-467.

10. Hallikainen, M., 1983, Remote Sensing of the Water Equivalent of Snow Cover by Passive Microwave Satellite Observations, Digest of the 3rd IEEE Intl. Geoscience and Remote Sensing Symp., San Francisco, CA, 31 August - 2 September.

11. Cumming, W., 1952, The Dielectric Properties of Ice and Snow at 3.2 Centimeters, J. Appl. Phys., Vol. 23, No. 7, pp. 768-773.

12. Sweeney, B. D., and S. C. Colbeck, 1974, Measurements of the Dielectric Properties of Wet Snow Using a Microwave Technique, Research Report 325, U.S. Army Cold Regions Research and Engineering Laboratory, Hanover, NH.

13. Tabarias, J., D. Sagnet, and J. Chilo, 1978, Determination of the Water Content of Snow from the Study of Electromagnetic Wave Propagation in the Snow Cover, J. Glac., Vol. 20, No. 84, pp. 585-592.

14. Linlor, W. I., 1980, Permittivity and Attenuation of Wet Snow Between 4 and 12 GHz, J. Appl. Phys., Vol. 51, pp. 2811-2816.

15. Nyfors, E., 1983, On the Dielectric Properties of Dry Snow in the 800 MHz to 13 GHz Region, Report S135, Helsinki University of Technology, Radio laboratory, Otaniemi, Finland.

16. Glen, J. W., and P. G. Paren, 1975, The Electrical Properties of Snow and Ice, J. Glac., Vol. 15, pp. 15-38.

17. Colbeck, S. C., 1980, Liquid Distribution and the Dielectric Constant of Wet Snow, NASA Workshop on Microwave Remote Sensing of Snowpack Properties, NASA CP2153, Fort Collins, CO, May 20-22.

18. Ambach, W., and A. Denoth, 1980, The Dielectric Behavior of Snow: A Study Versus Liquid Water Content, NASA Workshop on Microwave Remote Sensing of Snowpack Properties, NASA CP-2153, Fort Collins, CO, May 20-22.

19. Tiuri, M., and H. Schultz, 1980, Theoretical and Experimental Studies of Microwave Radiation from a Natural Snow Field, NASA Workshop on Microwave Remote Sensing of Snowpack Properties, NASA CP-2153, Fort Collins, CO, May 20-22.

20. Hallikainen, M., and F. T. Ulaby, 1983, A Free-Space System for Dielectric Measurements in the 3-18 GHz Frequency Range, RSL Technical Report 545-3, University of Kansas Center for Research, Inc., Lawrence, KS.

21. Hallikainen, M., F. T. Ulaby, M. Abdelrazik, and D. R. Brunfeldt, 1984, A 37-GHz Free-Space System for Dielectric Measurements, RSL Technical Report 333-1, University of Kansas Center for Research, Inc., Lawrence, KS.

22. Von Hippel A. (ed.), 1954, Dielectric Materials and Applications, M.I.T. Press, Cambridge, MA.

23. Ambach, W., and A. Denoth, 1972, Studies on the Dielectric Properties of Snow, Zeitschrift für Gletscherkunde und Glazialgeologie, Bd VIII, Heft 1-2, pp. 113-123.

24. Evans, S., 1965, Dielectric Properties of Ice and Snow - A Review, J. Glac., Vol. 5, No. 42, pp. 773-792.

25. Hallikainen, M., 1978, Measured Permittivities of Snow and Low-Salinity Sea Ice for UHF Radiometer Applications, Swedish National Convention on Radio Science, Stockholm, March 29-31.

26. Tiuri, M., A. Sihvola, and E. Nyfors, 1983, The Complex Dielectric Constant of Snow at UHF Frequencies, EARSeL WG on Microwave Remote Sensing of Snow, Snow Wetness Workshop, Berne, Switzerland.

27. Polder, D., and J. H. Van Santen, 1946, The Effective Permeability of Mixtures of Solids, Physica, Vol. 12, pp. 257-271.

28. Stiles, W. H., and F. T. Ulaby, 1981, Dielectric Properties of Snow, RSL Technical Report 527-1, University of Kansas Center for Research, Inc., Lawrence, KS.

29. Tinga, W. R., W. A. G. Voss, and D. F. Blossey, 1973, Generalized Approach to Multiphase Dielectric Mixture Theory, J. Appl. Phys., Vol. 44, pp. 3897-3902.

30. de Loor, G. P., 1964, Dielectric Properties of Heterogeneous Mixtures with a Polar Constituent, Appl. Sci. Res., Section B, Vol. 11, pp. 310-319.

31. Birchak, J. R., C. G. Gardner, J. E. Hipp, and J. M. Victor, 1974, High Dielectric Constant Microwave Proves for Sensing Soil Moisture, Proc. IEEE, Vol. 62, No. 1, pp. 93-98.

32. H. J. Eom, K. K. Lee, and A. K. Fung, 1983, Microwave Emission from an Irregular Snow Layer, Remote Sensing of Environment, Vol. 13, pp. 423-437.

Table 1. Summary of Microwave Dielectric Measurements of Snow.

Frequency (GHz)	Snow Density (g/cm^3)	Liquid Water Content (%)	Crystal Size Diameter (mm)	Temperature T(°C)	Reference and Year
9.375	0.34 - 0.916	0	not reported	-18 to 0	Cumming [11] 1952
9.375	0.38, 0.76	0-1.2	not reported	0	Cumming [11] 1952
6	0.6	0-24.4	not reported	0	Sweeny and Colbeck [12] 1974
9.4	0.5	0-9.0	not reported	0	Tabarias et al. [13] 1978
4-12	0.30 - 0.60	0-12.0	0.1 - 1.0	0	Linlor [14] 1980
0.8-13	0.07 - 0.53	0	not reported	-30 to -5	Nyfors [15] 1983

Table 2. Effect of the Shape of Water Inclusions to the Capability of the Two-Phase Polder and Van Santen Model to Describe the Dielectric Behavior of Snow in the 3- to 37-GHz Range (995 Data Points).

Model	Shape of Water Inclusions Symmetrical, A_{wi} Optimized Using ε_{ws}' Data		Shape of Water Inclusions Symmetrical, A_{wi} Optimized Using ε_{ws}'' Data		Shape of Water Inclusions Nonsymmetrical, Independent of Water Content of Snow, A_{wi} Optimized Using ε_{ws}'' Data		Shape of Water Inclusions Nonsymmetrical, Depends on Water Content of Snow, A_{wi} Optimized Using ε_{ws}'' Data	
Parameter	ε_{ws}'	ε_{ws}''	ε_{ws}'	ε_{ws}''	ε_{ws}'	ε_{ws}''	ε_{ws}'	ε_{ws}''
A_{w1}	0.155		0.074		0.067			
A_{w2}	0.155		0.074		0.251		See Figure 9	
A_{w3}	0.690		0.852		0.682		for values of A_{wi}	
Residual Sum of Squares	7.965	25.079	64.246	4.702	8.592	2.997	4.399	2.611
Linear Correlation Coefficient	0.978	0.961	0.981	0.962	0.984	0.975	0.988	0.978
α', α''	1.001	1.791	0.700	0.957	1.116	0.989	1.025	0.996
β', β''	-0.012	0.031	0.398	0.020	-0.160	0.005	-0.040	-0.003

$$\varepsilon_{ws}'(\text{obs}) = \alpha' \varepsilon_{ws}'(\text{pred}) + \beta'$$

$$\varepsilon_{ws}''(\text{obs}) = \alpha'' \varepsilon_{ws}''(\text{pred}) + \beta''$$

Table 3. Effect of the Shape of Water Inclusions to the Capability of the Three-Phase Polder and Van Santen Model to Describe the Dielectric Behavior of Snow in the 3- to 37-GHz Range (995 Data Points).

Model	Shape of Water Inclusions Symmetrical, A_{wi} Optimized Using ε_{ws}' Data		Shape of Water Inclusions Symmetrical, A_{wi} Optimized Using ε_{ws}'' Data		Shape of Water Inclusions Nonsymmetrical, A_{wi} Optimized Using ε_{ws}'' Data		Shape of Water Inclusions Nonsymmetrical, A_{wi} Optimized Using ε_{ws}'' Data	
Parameter	ε_{ws}'	ε_{ws}''	ε_{ws}'	ε_{ws}''	ε_{ws}'	ε_{ws}''	ε_{ws}'	ε_{ws}''
A_{w1}	0.189		0.084		0.047			
A_{w2}	0.189		0.084		0.372		See Figure 10	
A_{w3}	0.622		0.832		0.581		for values of A_{wi}	
Residual Sum of Squares	7.581	22.432	66.321	3.853	13.566	3.451	4.210	2.813
Linear Correlation Coefficient	0.980	0.975	0.982	0.969	0.989	0.971	0.988	0.967
α', α''	0.960	1.772	0.675	0.968	1.193	0.981	0.804	0.868
β', β''	0.081	0.023	0.458	0.017	-0.292	0.009	0.298	0.006

$$\varepsilon_{ws}'(\text{obs}) = \alpha' \varepsilon_{ws}'(\text{pred}) + \beta'$$

$$\varepsilon_{ws}''(\text{obs}) = \alpha'' \varepsilon_{ws}''(\text{pred}) + \beta''$$

Table 4. Capability of the Models to Predict the Dielectric Constant of Snow ε_{ws}' in the 3- to 37-GHz Range. Number of Data Points is 107 at 6 GHz and at 12 GHz, 63 at 37 GHz, and 995 in the 3- to 37-GHz range.

Parameter	Model Frequency (GHz)	Two-Phase Polder and Van Santen	Three-Phase Polder and Van Santen	Confocal Ellipsoidal	Debye-Like	Refractive (k=0.083)	Linlor-Like
Residual Sum of Squares	6	0.444	0.488	7.295	0.755	1.268	0.855
	12	0.417	0.365	1.973	0.674	0.943	0.570
	37	0.153	0.137	0.653	0.310	1.007	0.183
	3-37	4.399	4.210	33.761	8.462	11.963	5.826
Linear Correlation Coefficient	6	0.992	0.991	0.947	0.987	0.987	0.987
	12	0.987	0.989	0.959	0.983	0.982	0.983
	37	0.977	0.980	0.979	0.977	0.962	0.975
	3-37	0.988	0.988	0.943	0.977	0.968	0.984
α'	6	1.058	0.822	1.371	0.977	1.127	1.055
	12	1.092	0.825	1.145	1.097	0.933	1.022
	37	0.950	0.768	1.051	1.136	0.711	0.958
	3-37	1.025	0.804	1.217	0.960	0.985	1.009
β'	6	-0.074	0.294	-0.453	0.040	-0.178	-0.071
	12	-0.151	0.257	-0.169	-0.154	0.064	-0.050
	37	0.082	0.359	0.014	-0.166	0.410	0.064
	3-37	-0.040	0.298	-0.256	0.067	0.00	-0.016

$$\varepsilon_{ws}'(\text{obs}) = \alpha'\varepsilon_{ws}'(\text{pred}) + \beta'$$

Table 5. Capability of the Models to Predict the Loss Factor of Snow ε_{ws}'' in the 3- to 37-GHz Range. Number of Data Points is 107 at 6 GHz and at 12 GHz, 63 at 37 GHz, and 995 in the 3- to 37-GHz range.

Parameter	Model Frequency (GHz)	Two-Phase Polder and Van Santen	Three-Phase Polder and Van Santen	Confocal Ellipsoidal	Debye-Like	Refractive (k=0.369)
Residual Sum of Squares	6	0.273	0.318	5.873	0.587	0.980
	12	0.237	0.270	3.083	0.373	0.386
	37	0.070	0.048	0.160	0.266	0.268
	3-37	2.611	2.813	31.264	4.932	6.493
Linear Correlation Coefficient	6	0.981	0.978	0.836	0.960	0.962
	12	0.983	0.981	0.874	0.975	0.975
	37	0.981	0.987	0.958	0.975	0.975
	3-37	0.978	0.967	0.799	0.957	0.944
α''	6	1.018	0.980	2.795	1.031	1.239
	12	0.995	0.847	1.715	0.966	0.958
	37	0.870	0.749	1.062	1.367	0.819
	3-37	0.996	0.868	1.551	0.995	0.975
β''	6	0.005	0.009	-0.025	0.002	0.002
	12	-0.004	0.004	-0.027	-0.003	-0.005
	37	-0.011	-0.008	-0.019	-0.005	-0.010
	3-37	-0.003	0.006	0.008	0.003	0.005

$$\varepsilon_{ws}''(\text{obs}) = \alpha''\varepsilon_{ws}''(\text{pred}) + \beta''$$

Table 6. Linear Expressions For the Water Content Dependence of $\Delta\varepsilon_{ws}'$ and ε_{ws}'' Between 3 and 37 GHz (Modified Debye-Like Model).

$$\Delta\varepsilon_{ws}' = k_1 m_v \quad ; \quad 0 < m_v < 12\ \%$$

$$\varepsilon_{ws}'' = k_2 m_v$$

Frequency (GHz)	k_1	k_2
3	0.137	0.044
4	0.132	0.054
6	0.117	0.067
8	0.105	0.073
10	0.092	0.074
12	0.081	0.072
14	0.072	0.069
16	0.065	0.066
18	0.058	0.063
37	0.033	0.049

Table 7. Properties of Snow Types Used for Scattering Loss Measurements at 37 GHz.

Snow Type Abbreviation	Approximate Particle Diameter (mm)	Average Snow Density (g/cm^3)	Snow Type Description
(83/1)	1.4	0.354	Refrozen snow. The snow cover had already gone through the melting-refreezing process. Ice was continuous throughout the sample.
(83/2)	1.4	0.432	Refrozen snow. The snow sample consisted of separate particles. This was generated by mechanically handling (83/1) snow to break the continuous ice structure.
(83/3)	1.0	0.321	Newly-fallen snow that had not undergone the melt-refreeze process.
82	1.5	0.385	Old snow. Had been stored for one year in a freezer at -20°C. The ice structure was continuous in these samples. However, it was mechanically broken before the measurement causing separate particles.

Table 8. Comparison of Measured and Calculated (Mie Scattering) Extinction Coefficients for Dry Snow Types (Table 7) at 37 GHz.

Snow Type	κ_e (dB/m) Measured	κ_e (dB/m) Calculated
(83/1)	55.4	80.2
(83/2)	49.1	97.8
(83/3)	33.0	32.5
82	56.5	89.5